Loss spectra of graphite-related systems: A multiwall carbon nanotube, a single-wall carbon nanotube bundle, and graphite layers

F. L. Shyu[1] and M. F. Lin[2,*]
[1]*Department of Electronics Engineering, Fortune Institute of Technology, Kaohsiung 842, Taiwan, The Republic of China*
[2]*Department of Physics, National Cheng Kung University, Tainan 701, Taiwan, The Republic of China*
(Received 11 February 2000)

The π-electron excitations are studied for a multiwall carbon nanotube, a single-wall carbon nanotube bundle with finite nanotubes, and graphite layers. The loss spectra of the nanotube systems exhibit several plasmon peaks. The most prominent one is the π plasmon, and the others are the interband plasmons. The latter are absent in graphite layers. The π plasmon depends on the number of carbon nanotubes or graphite layers (N), the transferred momentum (q), and the transferred angular momentum (L). The intertube or interlayer Coulomb interactions clearly enhance π-plasmon frequency and oscillator strength as N increases. A multiwall carbon nanotube can exhibit L-decoupled π plasmons. For the $L=0$ π plasmon, the multiwall nanotube behaves like graphite layers, but not like a single-wall carbon nanotube bundle. The radius dependence is negligible for a multiwall nanotube, while it is strong for a single-wall nanotube bundle. Furthermore, the former exhibits stronger collective excitations, higher π-plasmon frequency, and relatively rapid increase of plasmon frequency with q. The calculated results are compared with experimental measurements.

I. INTRODUCTION

Iijima reported observation of multiwall carbon nanotubes (MWNT's) in 1991.[1] The number of nanotubes in a multiwall carbon nanotube can vary from $N=2$ to ~ 100.[1–5] The smallest inner radius is $r\sim 5$ Å and the largest outer radius is $r\sim 300$ Å. Single-wall carbon nanotubes (SWNT's), with a small radius $r\sim 3.5-20$ Å, have also been produced.[6–8] When they are closely packed together, a carbon nanotube bundle is formed. There are about 10–600 single-wall nanotubes in a carbon nanotube bundle.[9–12] Multiwall carbon nanotubes and carbon nanotube bundles are closely related to graphite layers. These graphite-related systems might exhibit similar physical properties. For example, π-electronic collective excitations (π plasmons) exist in carbon nanotubes[2,3,11,12] and graphite.[13–15] In this work, we study primarily the π-electronic excitations in a multiwall carbon nanotube, a single-wall carbon nanotube bundle with finite nanotubes, and graphite layers. The dependence of the π plasmons on the number of carbon nanotubes or graphite layers, the transferred momentum (q), the transferred angular momentum (L), and the nanotube geometry (radius r and chiral angle θ) is investigated. The graphite-related systems are compared with one another. Comparison with experimental measurements[2,12,16] is discussed.

Electron-energy-loss spectroscopy (EELS) can be utilized to observe π plasmons in graphite-related systems. There have been some measurements on multiwall carbon nanotubes.[2,3,11] Kuzuo *et al.*[2] reported that multiwall carbon nanotubes with $N\sim 21-44$ exhibit a pronounced π-plasmon peak in the loss spectrum at $\omega_p\sim 5.1-5.4$ or $\sim 6.2-6.4$ eV. That is to say, there are two kinds of π-plasmon mode in multiwall carbon nanotubes. Kuzuo, Terauchi and Tanaka[12] also measured the loss spectra of a single-wall carbon nanotube bundle with $N\sim 600$. A 5.8 eV π plasmon is found to exist in the finite-size nanotube bundle. Friedlein *et al.*[16] recently measured q-dependent loss spectra for multiwall carbon nanotubes with $N\sim 12$, single-wall nanotube bundles with $N\sim 10-100$, and graphite layers. Their π-plasmon frequencies depend linearly on momentum at large q. The q dependence of the π-plasmon frequency is stronger for multiwall carbon nanotubes or graphite layers than for single-wall nanotube bundles. Moreover, the former have higher π-plasmon frequencies except at very small q. On the theoretical side, the π plasmons in a single-wall carbon nanotube or an infinite single-wall carbon nanotube bundle have been studied within the random-phase approximation (RPA).[17] Due to the cylindrical symmetry, a single-wall carbon nanotube can exhibit L-decoupled π plasmons with strong q-dependent dispersion relations.[18] The L-decoupled plasmon modes are expected to be present also in a multiwall carbon nanotube. For an infinite single-wall carbon nanotube bundle,[19] the π plasmon is strongly affected by the magnitude and direction of the transferred momentum.

The graphite-related systems are modeled as superlattice systems. Graphite has highly anisotropic conductivity. That parallel to the graphite planes is several orders of magnitude higher than that along the c axis ($\sigma_a/\sigma_c\sim 3\times 10^3$).[20] Hence the π-electron states are mainly localized on the graphite planes. The covalent bonds in a graphite layer are much stronger than the van der Waals interactions between graphite layers. When the weak interlayer interactions are taken into account, they modify the π-band structure near the Fermi level. A graphite layer is a zero-gap semiconductor, and graphite is a semimetal with a small number of free carriers ($\sim 10^{19}e/\mathrm{cm}^3$). Nanotube systems are similar, e.g., multiwall carbon nanotubes.[21,22] The weak interactions between graphite layers mainly affect the low-frequency (<0.1 eV),[23] but not the high-frequency π plasmon (>5 eV). The former is caused by the π-electron states near the K point (the corner of the hexagonal Brillouin zone), and the latter is associated with those near the M point (the middle point

between K and K'). A model in which the layered graphite is regarded as a two-dimensional (2D) superlattice should be a reasonable first approximation for the study of the high-frequency π-electron excitations. Graphite layers are independent of each other, while there are Coulomb interactions for electrons in different layers. This model had been successfully used to investigate high-frequency π-electron excitations in graphite, e.g., optical properties[24–27] and elementary excitations[28] at high frequencies. It could provide a reasonable explanation for the measured optical spectra[15] and loss spectra.[13,14] A single-wall carbon nanotube is only a graphite sheet rolled up in cylindrical form. The superlattice model is thus expected to be suitable for the π plasmons in multiwall carbon nanotubes and single-wall carbon nanotube bundles.

The tight-binding model[29,30] is used to calculate the π band and the RPA to evaluate the loss spectra of the graphite-related systems. The intertube or interlayer Coulomb interactions have a strong effect on the π-plasmon frequency and the oscillator strength of collective excitations. The study shows that the π plasmons in graphite layers behave like those in a multiwall carbon nanotube, but not like those in a single-wall carbon nanotube bundle. The calculated results can explain the π plasmons observed by EELS, the $\sim$5.1–5.4 or the $\sim$6.2–6.4 eV π plasmon in a multiwall carbon nanotube,[2] the 5.8 eV π plasmon in a single-wall carbon nanotube bundle,[12] and the q-dependent π-plasmon frequencies in graphite-related systems.[16]

This paper is organized as follows. In Sec. II, the dielectric response including the intertube or interlayer Coulomb interactions is calculated within the RPA. The loss spectra are studied for a multiwall carbon nanotube, a single-wall carbon nanotube bundle, and graphite layers in Sec. III. Concluding remarks are given in Sec. IV.

II. DIELECTRIC RESPONSE OF GRAPHITE-RELATED SYSTEMS

A cylindrical carbon nanotube can be built from a graphite sheet.[31] Its geometric structure is fully specified by a lattice vector $\mathbf{R}_{\mathbf{x}}=m\mathbf{a}_1+n\mathbf{a}_2$, where $\mathbf{a}_1$ and $\mathbf{a}_2$ are primitive lattice vectors of the graphite sheet, and m and n are integers. An (m,n) carbon nanotube has radius $r=|\mathbf{R}|/2\pi=b\sqrt{3(m^2+mn+n^2)}/2\pi$ and chiral angle $\theta=\tan^{-1}[-\sqrt{3}n/(2m+n)]$. $b=1.42$ Å is the C-C bond length. The π-band structures of a graphite layer and a single-wall carbon nanotube have been given for easy reference in the Appendix. The energy dispersions and the wave functions [Eqs. (A1)–(A5)] are used directly to calculate the dielectric response of graphite-related systems.

We first consider a multiwall carbon nanotube with N shells. The π electrons are localized on individual nanotubes. As a result of the cylindrical symmetry,[32–34] the transferred momentum and angular momentum are conserved in the electron-electron interactions. Electronic excitations have a well-defined (q,L,ω), and so does the dielectric response. An N-shell multiwall nanotube is assumed to be perturbed by a probing electron via the time-dependent potential $v^{\mathrm{ex}}(q,L,\omega)$. This external field induces charge fluctuations on all coaxial nanotubes. The screening charges build up the induced potential $v^{\mathrm{in}}(q,L,\omega)$. Within the RPA,[17] the induced potential is proportional to the effective potential, the proportionality coefficient having the response function. The effective potential $v^{\mathrm{eff}}(q,L,\omega)$ is the sum of the external potential and the induced potential from screening charges on all nanotubes. $v_i^{\mathrm{eff}}(q,L,\omega)$ on the ith shell is given by the linear relation[32–35]

$$\begin{aligned}\epsilon_0 v_i^{\mathrm{eff}}(q,L,\omega)&=v_i^{\mathrm{ex}}(q,L,\omega)+v_i^{\mathrm{in}}(q,L,\omega)\\&\equiv v_i^{\mathrm{ex}}(q,L,\omega)\\&\quad+\sum_{j=1}^{N}V_{ij}(q,L)v_j^{\mathrm{eff}}(q,L,\omega)\chi_j(q,L,\omega).\end{aligned}\tag{1}$$

ϵ_0 is the background dielectric constant contributed from high-energy excitations (other than those excitations within the π bands). $V_{ij}(q,L)=4\pi e^2 I_L(qr_<)K_L(qr_>)$ is the bare Coulomb interaction of two electrons on the ith and jth nanotubes, with radii r_i and r_j, respectively. I_L (K_L) is a modified Bessel function of the first (second) kind of order L. $r_<(r_>)$ represents the smaller (larger) of r_i and r_j. $v_j^{\mathrm{eff}}(q,L,\omega)\chi_j(q,L,\omega)$ is the screening charge density on the jth nanotube. The response function of the jth nanotube at $T=0$ is[18]

$$\chi_j(q,L,\omega)=\frac{-4}{(2\pi)^2}\sum_J\int dk_y\frac{E^c(J+L,k_y+q)-E^v(J,k_y)}{[E^c(J+L,k_y+q)-E^v(J,k_y)]^2-(\omega+i\Gamma)^2}\times\left|\langle J+L,k_y+q,c|e^{iL\phi'}e^{iqy}|J,k_y,v\rangle\right|^2,\tag{2a}$$

where

$$\left|\langle J+L,k_y+q_y,c|e^{iL\phi'}e^{iqy}|J,k_y,v\rangle\right|^2=\frac{1}{4}\left|1-\frac{H_{12}(J+L,k_y+q)H_{12}^*(J,k_y)}{|H_{12}(J+L,k_y+q)H_{12}^*(J,k_y)|}\right|^2.\tag{2b}$$

Γ is the energy width due to various deexcitation mechanisms. J and k_y in Eq. (2a) change with the nanotube geometry (r_j,θ_j). The response function describes the π-electronic excitations. Electrons are excited from the occupied π subbands to the unoccupied π^* subbands at $T=0$, i.e., they exhibit inter-π-band excitations. The excitation energy is denoted by $\omega_{vc}=E^c-E^v$. The product of the bare Coulomb interaction and the response function, $V_{ij}\chi_j$ in Eq. (1), determines the features of the π plasmon, e.g., its r dependence.

The external potential $v_i^{\rm ex}(q,L,\omega)$ is required for the study of the π-electronic excitations. From the recent measurements of plasmons,[36] the momentum resolution of EELS is $\Delta q \sim 0.06\,\text{Å}^{-1}$. The wave-packet width ($>1/\Delta q$) of the probing electron is much larger than the intertube distance. The density distribution of the probing electron can be roughly estimated to be uniform inside the system. Such an approximation might somewhat overestimate the π-plasmon frequency ($\sim 0.1\gamma_0$ at large N).[28] However, it does not affect the main features of the π plasmons. From the known external potential, we can obtain the effective potential $v_i^{\rm eff}(q,L,\omega)$ in Eq. (1) by solving an $N\times N$ matrix. According to the Fermi golden rule, the probability per unit time P that the probing electron transfers (q,L,ω) to the nanotube system is

$$P=\sum_{i=1}^{N} -\mathrm{Im}(\chi_i)|v_i^{\rm eff}|^2 \equiv \left\langle \sum_{i=1}^{N} v_i^{\rm ex}\right\rangle \mathrm{Im}\left(\frac{-1}{\epsilon}\right). \tag{3}$$

$-\mathrm{Im}(\chi_i)$ describes all inter-π-band excitation channels. The external Coulomb potential is screened by the π electrons in the system. The effective Coulomb potential experienced by the π electrons is $v_i^{\rm eff}$. $\langle\Sigma_{i=1}^{N} v_i^{\rm ex}\rangle$ is the average external potential. Equation (3) defines a dimensionless quantity $\mathrm{Im}(-1/\epsilon)$, which can be interpreted as the intensity of loss spectrum. It will be used to identify the π plasmon from the most prominent peak in the loss function. The dielectric function of an N-nanotube system can be defined as $\Sigma_j \epsilon_{ij} v_j^{\rm eff}=v_i^{\rm ex}$, i.e., $\epsilon_{ij}=\epsilon_0\delta_{ij}-V_{ij}\chi_j$. $\det(\epsilon_{ij})=0$ is not suitable for determining the π-plasmon frequency, since there are strong inter-π-band e-h excitations or Landan damping. Moreover, we cannot get the loss spectrum from ϵ_{ij}. ϵ_{ij} might not be useful in studying the π plasmons in graphite-related systems.

A finite-size bundle is made up of parallel, identical, single-wall carbon nanotubes. For convenience, carbon nanotubes are assumed to be located in accordance with a triangular lattice[9] with the smallest intertube distance $d=3.4\,\text{Å}$. The number of nanotubes in a closely packed nanotube bundle is $N=1,7,19,37,61$, etc. Here we focus only on the case that the external electric field is parallel to the nanotube axis. The transferred momentum is only along the nanotube axis for longitudinal dielectric response. The $L=0$ excitations in each nanotube predominate in the excitation spectrum, as indicated by results from an infinite nanotube bundle [Eq. (5)].[19] Other cases are very complicated, since the electronic excitations of different L's in separate carbon nanotubes are coupled with one another.

As for a multiwall carbon nanotube, the linear response approximation is used to get the relation between the effective potential and the external potential:

$$\epsilon_0 v_i^{\rm eff}(q,L=0,\omega)=v_i^{\rm ex}(q,L=0,\omega)+\sum_{j=1}^{N} V_{ij}(q,L=0)v_j^{\rm eff}(q,L=0,\omega)\times\chi_j(q,L=0,\omega), \tag{4a}$$

where the bare intertube Coulomb interaction is given by

$$V_{ij}(q,L=0)=2e^2\int_0^{2\pi}d\phi\int_0^{2\pi}d\phi' K_0\{q\sqrt{2r^2[1-\cos(\phi-\phi')]+d_{ij}^2-2rd_{ij}(\cos\phi-\cos\phi')}\}. \tag{4b}$$

d_{ij} is the distance between two nanotube centers. The loss spectrum $\mathrm{Im}(-1/\epsilon)$ is calculated from Eqs. (3) and (4). For an infinite nanotube bundle, the loss spectrum can be directly obtained from the dielectric function:[18]

$$\epsilon(q,\omega)=\epsilon_0-\frac{8\pi^2e^2}{q^2}N_a\chi(q,L=0,\omega), \tag{5}$$

where N_a is the nanotube number per area.

The π-electron response of graphite layers is calculated. A single graphite layer is a zero-gap semiconductor.[28,30] The π band is anisotropic in the plane. The excitation spectra depend on the magnitude (q) and direction (ϕ) of the transferred momentum. ϕ is the angle between the transferred momentum and the vector $\mathbf{\Gamma}$-$\mathbf{K}$, where the K point corresponds to the corner of the first Brillonin zone (see the Appendix).[31] $0°\leqslant\phi\leqslant 30°$ is sufficient to characterize the direction-dependent excitations because of the hexagonal symmetry. A study of graphite[28] indicates that the ϕ dependence of the π plasmons is weak at $q<1\,\text{Å}^{-1}$. $\phi=0°$ is used in this study.

When the interlayer e-e interactions among graphite layers are taken into account, the effective potential on the ith layer is given by

$$\epsilon_0 v_i^{\rm eff}(q,\phi=0°,\omega)=v_i^{\rm ex}(q,\phi=0°,\omega)+\sum_{j=1}^{N} V_{ij}(q)v_j^{\rm eff}\times(q,\phi=0°,\omega)\chi(q,\phi=0°,\omega). \tag{6}$$

$V_{ij}(q)=(2\pi e^2/q)\exp(-q|i-j|I_c)$ is the interlayer Coulomb interaction, where I_c is the interlayer distance. The response function of a single graphite layer is

$$\chi(q,\phi=0°,\omega)=\frac{-4}{(2\pi)^2}\int\int dk_x' dk_y' \frac{E^c(k_x'+q,k_y')-E^v(k_x',k_y')}{[E^c(k_x'+q,k_y')-E^v(k_x',k_y')]^2-(\omega+i\Gamma)^2}\times|\langle k_x'+q,k_y',c|e^{iqx'}|k_x',k_y',v\rangle|^2, \tag{7a}$$

where

$$|\langle k_x'+q,k_y',c|e^{iqx'}|k_x',k_y',v\rangle|^2 = \frac{1}{4}\left|1-\frac{H_{12}(k_x'+q,k_y')H_{12}^*(k_x',k_y')}{|H_{12}(K_x'+q,k_y')H_{12}^*(k_x',k_y')|}\right|^2. \tag{7b}$$

Equations (6) and (3) determine the excitation spectra of finite graphite layers. As to graphite with $N=\infty$, the electronic excitations are described by the dielectric function[28]

$$\epsilon(q,\phi=0°,\omega)=\epsilon_0-\frac{2\pi e^2\sinh(qI_c)}{q[\cosh(qI_c)-1]}\chi(q,\phi=0°,\omega). \tag{8}$$

III. LOSS SPECTRA

The calculations are principally based on the following parameters. The background dielectric constant[15] $\epsilon_0=2.4$ and the energy width $\Gamma=0.04\gamma_0$. The intertube distance of carbon nanotubes is $d=3.4$ Å,[1,37] and the interlayer distance of graphite layers is $I_c=3.35$ Å.[38] The (10,10) armchair nanotube is chosen as the innermost nanotube of a multiwall nanotube, or the single-wall nanotube in a nanotube bundle.[9] The radius and chiral angle of the (10,10) nanotube are, respectively, $r=6.67$ Å and $\theta=-30°$. The π-band structure is given in Eq. (A5). Moreover, all nanotubes in a multiwall nanotube are chosen to be (m,m) armchair nanotubes. Effects due to changes in chiral angles will be proved to be negligible. A multiwall nanotube and a finite-size nanotube bundle might have the same size, e.g., the former with $N=11$ [Fig. 2(a) below] and the latter with $N=19$ [Fig. 2(b)]. The calculated results are given in the following subsections.

A. A multiwall carbon nanotube

Figure 1(a) presents the loss spectra of multiwall carbon nanotubes at $L=0$, $q=0.1$ Å^{-1}, and different N's. Each excitation spectrum exhibits several peaks. Such peak structures are related to 1D subbands with divergent density of states. They can be considered as plasmons. The most prominent peak is identified as the π plasmon. As has been discussed,[18] the π plasmon is induced by inter-π-band excitations from the concave-upward subbands at $E^v(k_y)\sim-\gamma_0$ to the concave-downward subbands at $E^c(k_y+q)\sim\gamma_0$ (see the Appendix). The π plasmon is the quantum of collective π-electron oscillations. This plasmon also exists in graphite layers [see Fig. 4(b) below]. The plasmon frequency and oscillator strength clearly increase as N increases. That is to say, the π-electronic collective excitations are obviously enhanced by intertube Coulomb interactions. We also noted that the loss spectra are almost independent of the nanotube number for large N, e.g., $N>50$. The main reason is that the bare intertube Coulomb interaction $[V_{ij}(q,L]$ is very weak at large intertube distance. The other peaks in the loss spectra are associated with inter-π-band excitations except the above-mentioned excitations at $\omega\sim2\gamma_0$. They are called interband plasmons.[39] These plasmons do not exist in graphite owing to the absence of 1D subbands. The number of inter-π-band excitation channels increase with the nanotube radius or the number of 1D subbands; therefore, there are more interband different nanotubes reduces the oscillator strength of the interband plasmons. However, the mixing effect hardly affects the interband plasmon frequencies. This study is mainly focused on the features of the π plasmons.

A multiwall carbon nanotube can exhibit L-decoupled loss spectra. The $L=1$ loss spectra are shown in Fig. 1(b) at $q=0.1$ Å^{-1} and different N's. The loss spectra are similar for different L's, as seen in Figs. 1(b) and 1(a). The similarities include the most pronounced π-plasmon peak in each loss spectrum, and the enhancement of plasmon frequency and oscillator strength by intertube Coulomb coupling. The $L=0$ π plasmon corresponds to collective π-electron oscillations along the nanotube axis. But for the $L\neq0$ π plasmons

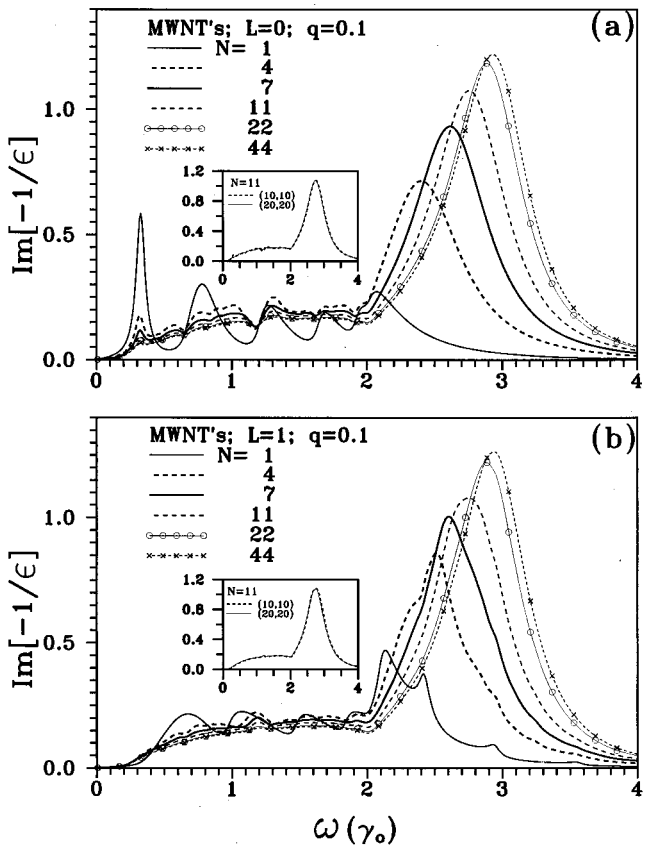

FIG. 1. (a) The loss spectra are shown for multiwall carbon nanotubes with different N's at $L=0$ and $q=0.1$. The (10,10) nanotube is the innermost nanotube of the multiwall nanotubes. The unit of q is Å^{-1}, here and henceforth. (b) Same plot as (a), but shown at $L=1$. The (20,20) nanotube is also chosen as the innermost nanotube. The calculated results are shown in the insets for comparison.

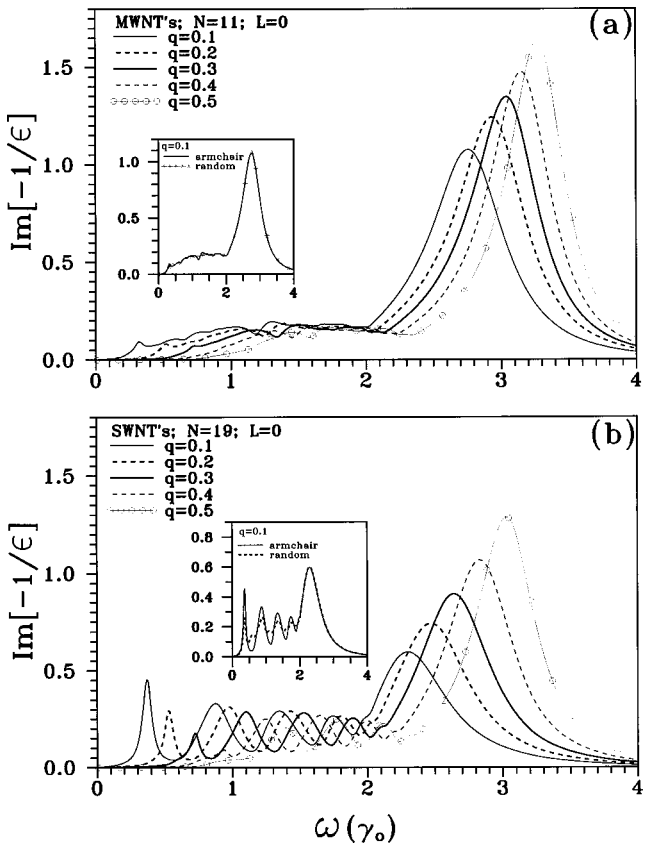

FIG. 2. (a) The loss spectra are shown for a multiwall carbon nanotube at $N=11$, $L=0$, and different q's. All carbon nanotubes are armchair nanotubes with $\theta=-30°$. (b) Same plot as (a), but shown for a single-wall carbon nanotube bundle at $N=19$. These two systems have the same size. Also shown in the insets are the results for carbon nanotubes with random chiral angles.

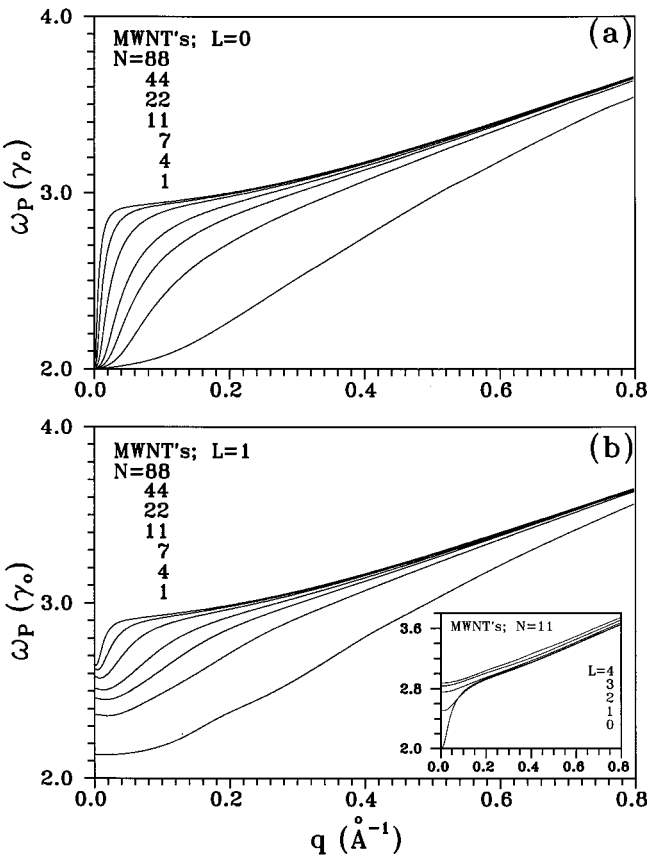

FIG. 3. The momentum-dependent π-plasmon frequencies of multiwall carbon nanotubes with different N's. They are shown for (a) the $L=0$ mode and (b) the $L=1$ mode. Also shown in the inset of (b) are the π-plasmon frequencies of different L's for an $N=11$ multiwall carbon nanotube.

there are transverse plasma oscillations in addition to longitudinal plasma oscillations. The inter-π-band excitation energy increases with increases L, and so does the π-plasmon frequency. $\omega_{vc}(L)$ is lower for larger carbon nanotubes. Consequently, the frequency differences among the L-decoupled plasmons become small as N grows.

In addition to N and L, the loss spectra are strongly affected by q. Figure 2(a) shows the loss spectra of the $N=11$ multiwall nanotube at $L=0$ and different q's. ω_p clearly increases with q. This result directly reflects π-band characteristic, the strong wave-vector dependence. The q dependence of the π plasmon means that the collective plasma oscillations along the nanotube axis behave like a propagating wave, with a wavelength $2\pi/q$.

Carbon nanotubes in a multiwall nanotube can have different chiral angles. θ's of the coaxial nanotubes are randomly chosen. The π-plasmon peaks in the loss spectra, as shown in the inset of Fig. 2(a), are independent of chiral angle. All carbon nanotubes have concave-upward subbands at $E^{v}\sim-\gamma_0$. Furthermore, the density of states is almost the same for carbon nanotubes with different θ's. These two π-band features can explain the negligible θ dependence. We change the inner radius of a multiwall nanotube to examine the r dependence. For the $L=0\,\pi$ plasmons, the plasmon peaks are hardly affected by the nanotube radius, e.g., the $L=0$ loss spectra shown in the inset of Fig. 1(a). This result remains true for any N. The π-plasmon peak in the loss spectrum is mainly determined by the magnitude of the bare Coulomb interaction [V_{ij} in Eq. (1)] and the excitation channels and the inter-π-band excitation energy included in the response function [χ_j in Eq. (2a)]. The Coulomb interaction decreases with nanotube radius, while the response function exhibits the opposite behavior. The weaker interaction just cancels with stronger response function, which thus leads to negligible r dependence. Very weak r dependence. is also obtained for the $L=1\,\pi$ plasmon, as shown in the inset of Fig. 1(b). However, the r dependence might be strong at $N\leqslant 7$ and $L\geqslant 3$. Roughly speaking, the dependence of the π plasmon on the nanotube geometry is weak except at small N and large L.

The dispersion relation of the $L=0\,\pi$ plasmon frequency with momentum is shown in Fig. 3(a) at different N's. ω_p approaches a finite value $2\gamma_0$ at $q\to 0$, when the nanotube number is finite. This result further illustrates that the π plasmon is associated with the inter-π-band excitations of the concave-upward-subbands at $E^{v}(k_y)\sim-\gamma_0$. The π plasmon is an optical plasmon because $\omega_p(q=0,L=0)=2\gamma_0$. At small q, ω_p grows rapidly with q, and the N dependence of ω_p is strong. On the other hand, at large q, ω_p exhibits linear q dependence, and the N dependence of ω_p becomes weak. Whether ω_p strongly depends on N is mainly determined by the intertube Coulomb interactions.

The $L=1\pi$ plasmon frequencies of multiwall nanotubes are shown in Fig. 3(b). There are several important differences between $L=1$ and $L=0$ plasmons. $\omega_p(q,L=1)$ is the oscillation frequency of mixed plasma oscillations parallel and perpendicular to the nanotube axis, while $\omega_p(q,L=0)$ is that of only the longitudinal plasma oscillations. At $q=0$, $\omega_p(L=1)$ differs appreciably from $\omega_p(L=0)$ $(=2\gamma_0)$. The former is higher than $2\gamma_0$, and it increases with N. Moreover, at small q, the q dependence of ω_p is weaker for the $L=1\pi$ plasmon. As to other $L\neq 0$ plasmons, the q-dependent plasmon frequencies are similar to that of the $L=1$ plasmon, e.g., the ω_p's of the L-decoupled plasmons shown in the inset of Fig. 3(b). Also note that all π plasmons are optical plasmons, and the q dependence of ω_p is linear at large q.

The π-plasmon frequencies obtained from the tight-binding model depend on the value of the resonance integral. $\gamma_0=3.033\,\mathrm{eV}$ has been used[29] to evaluate the π-plasmon frequencies in previous studies.[18,19] This value is suitable only when the overlap integral ($s_{pp\pi}$ in Ref. 29) is included in the calculations of the π and σ bands. $\gamma_0\sim 2.6-2.7\,\mathrm{eV}$ is used in other tight-binding calculations.[40–42] Estimations obtained from comparison between the tight-binding model and the local-density-functional approach put $\gamma_0\sim 2.4-2.5\,\mathrm{eV}$.[43,44] The reasonable range of γ_0 seems to be 2.4–2.7 eV. This range is the same as that of graphite.[45] $\gamma_0=2.5\,\mathrm{eV}$, as employed for graphite,[28] will be used to explain the measured π-plasmon frequencies of the graphite-related systems.

For multiwall nanotubes with $N=21-44$, the $L=0$ and $L=1$ plasmon frequencies are, respectively, $\omega_p(L=0)=5-6\,\mathrm{eV}$ and $\omega_p(L=1)=6.4-6.6\,\mathrm{eV}$ at $q=0-0.01\,\text{Å}^{-1}$. The average values are $\omega_p(L=0)=5.5\,\mathrm{eV}$ and $\omega_p(L=1)=6.5\,\mathrm{eV}$. The calculated results are consistent with the measured π-plasmon frequencies,[2] $\sim$5.2–5.4 and $\sim$6.2–6.4 eV. The consistency suggests that there are $L=0$ and $L=1\pi$ plasmons in the experimental loss spectra. The detailed q dependence of the measured π-plasmon frequency is needed for a complete comparison. The q-dependent plasmon frequencies were recently measured by Friedlein *et al.*[16] for a multiwall nanotube with $N\sim 12$. $\omega_p\sim 5.1\,\mathrm{eV}$ at $q=0.02\,\text{Å}^{-1}$. At small q, ω_p rapidly increases with q. Moreover, the q dependence of ω_p is linear at large q. These features are well explained by the calculated $L=0\,\pi$ plasmon frequencies [Fig. 3(a)]. The q dependence of the L-decoupled π plasmons needs further experimental verification.

B. A single-wall carbon nanotube bundle with finite nanotubes

The loss spectra of single-wall carbon nanotube bundles are shown in Fig. 4(a) at $q=0.1\,\text{Å}^{-1}$ and different N's. Each spectrum exhibits a pronounced π-plasmon peak. This peak comes from the superposition of the $L=0$ collective excitations in all carbon nanotubes. The π-plasmon frequency and the oscillator strength clearly increase with nanotube number. The longitudinal plasma oscillations on different carbon nanotubes are coupled by the intertube Coulomb interactions. The in-phase plasma oscillations lead to enhancement of π-plasmon frequency and oscillator strength.

The product of the intertube Coulomb interaction and the response function is obviously reduced by increasing the nanotube radius. Therefore, the π-plasmon frequency and oscillator strength decrease as r increases [inset in Fig. 4(a)]. The r dependence is strong for a nanotube bundle, while it is negligible for a multiwall nanotube [inset in Fig. 1(a)]. The main reason is that the intertube Coulomb interaction of the former is much weaker than that of the latter. This might also explain why a finite-size nanotube bundle exhibits lower π-plasmon frequency and weaker oscillator strength [Fig. 2(b)] than a multiwall nanotube [Fig. 2(a)]. A nanotube bundle[9] might be composed of single-wall nanotubes with different chiral angles.[46–48] θ affects the low-frequency interband plasmons, but not the π plasmon [inset in Fig. 2(b)]. A similar result is obtained for a multiwall nanotube [inset in Fig. 2(a)]. The θ dependence of the π plasmon is insignificant for all nanotube systems.

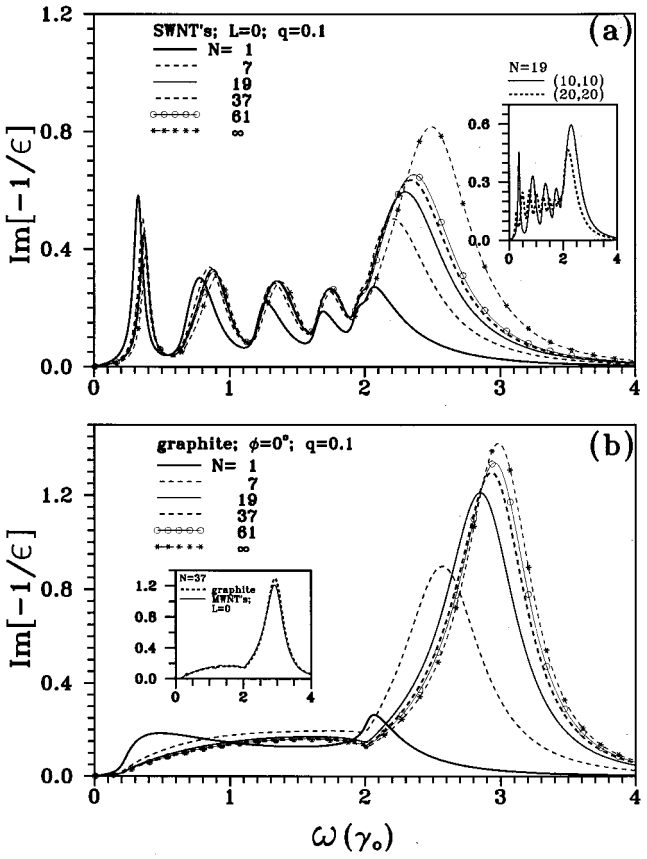

FIG. 4. (a) The loss spectra are shown for single-wall carbon nanotube bundles at $L=0$, $q=0.1$, and different N's. (b) Same plot as (a), but shown for graphite layers at $\phi=0°$ and $q=0.1$.

The q-dependent π-plasmon frequencies of a single-wall nanotube bundle are shown in Fig. 5(a) at $L=0$ and different N's. At small q, the q dependence of ω_p becomes stronger as N increases. ω_p is equal to $2\gamma_0$ at $q\to 0$ for finite N, while it is $\sim 2.5\gamma_0$ for $N=\infty$. This difference is because the Coulomb interactions have the 1D [Eq. (4b)] and 3D [Eq. (5)] forms, respectively, for finite N and $N=\infty$. At large N, much computer time is needed to get the q-dependent π-plasmon frequency, e.g., for the $N\sim 600$ nanotube bundle used in the experiments.[12] The π-plasmon frequency is $\omega_p=5-5.8\,\mathrm{eV}$ at $q=0-0.02\,\text{Å}^{-1}$. The measured 5.8 eV π plasmon should correspond to the $L=0\,\pi$ plasmon at very small q.

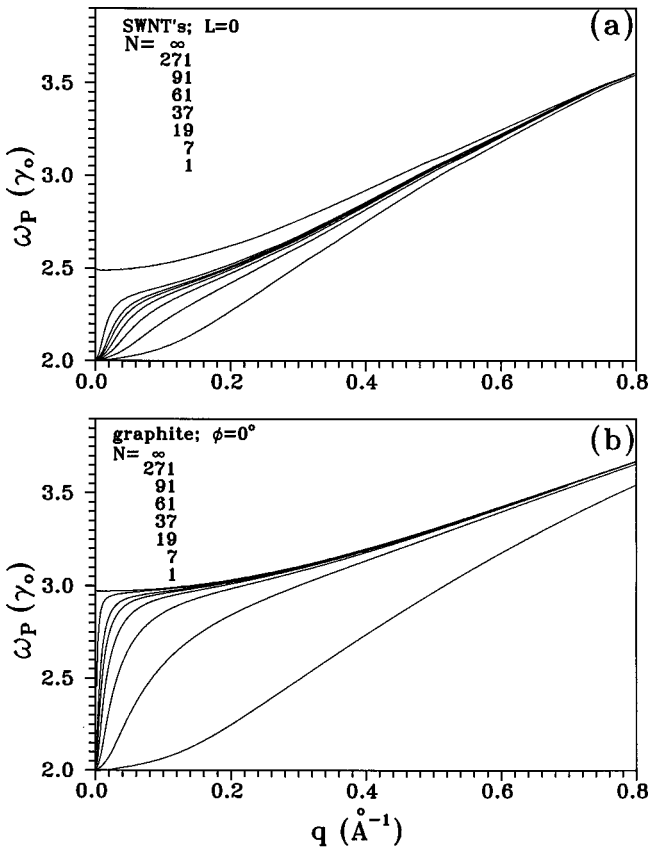

FIG. 5. The momentum-dependent π-plasmon frequencies are shown at different N's for (a) single-wall carbon nanotube bundles and (b) graphite layers.

The main similarities between a single-wall nanotube bundle and a multiwall nanotube include $\omega_p(q=0,L=0)=2\gamma_0$ for finite N and the linear q dependence of ω_p at large q [Figs. 5(a) and 3(a)]. On the other hand, there are two important differences. The single-wall nanotube bundle has lower π-plasmon frequencies, and it exhibits weaker q dependence at small q. In addition, when the nanotube number of the single-wall nanotube bundle is much larger than that of the multiwall nanotube, the former has higher plasmon frequency at $q \leqslant 0.03\,\text{Å}^{-1}$. The similarities or differences between these two systems can explain the experimental measurements.[16]

C. Graphite layers

Figure 4(b) shows the loss spectra of graphite layers at $\phi=0°$, $q=0.1\,\text{Å}^{-1}$, and different N's. There are only e-h excitations at $\omega<2\gamma_0$. The π-plasmon peak is induced by the inter-π-band excitations of the states near the M point (see the Appendix).[28] The interlayer Coulomb interactions clearly enhance the π-plasmon frequency and the oscillator strength as N increases. Graphite layers exhibits higher π-plasmon frequency and stronger oscillator strength compared with single-wall nanotube bundles [Fig. 4(a)]. However, graphite layers and multiwall nanotubes have almost the same π-plasmon peak at $L=0$, e.g., the loss spectra shown in the inset of Fig. 4(b). The π plasmons in graphite layers or multiwall nanotubes are relatively easily observed in experimental measurements.

The relationship between graphite and multiwall nanotubes deserves a closer investigation. That graphite layers do not have the interband plasmons and the $L\neq 0\,\pi$ plasmons is the most important difference. On the other hand, the π plasmons in graphite layers completely correspond to the $L=0\,\pi$ plasmons in a multiwall carbon nanotube. The main reasons are as follows. A single-wall carbon nanotube has concave-upward subbands at $E^v(k_y=0)\sim-\gamma_0$. Such subbands are sampled from the states near the M point of a graphite layer. These two kinds of state are the critical points in energy–wave-vector space.[28,18] The inter-π-band excitations due to them induce π plasmons. The q-dependent excitation energies, which are included in the response functions [Eqs. (2a) and (7a)], are the same for these two systems at $L=0$. The interlayer distance[38] ($I_c=3.35\,\text{Å}$) is very close to the intertube distance ($d=3.4\,\text{Å}$).[1,37] Moreover, the product of the response function and the interlayer or intertube Coulomb interaction is almost equal for the two systems at $\omega>2\gamma_0$. Graphite layers and multiwall nanotubes thus exhibit similar π plasmons at $L=0$ and various N's. They have identical π-plasmon frequencies. For finite N, the π-plasmon frequencies rapidly increase from $2\gamma_0$ at small q and display linear q dependence at large q [Figs. 5(b)/3(a)]. The $L=0\,\pi$ plasmon frequencies of an infinite multiwall nanotube can be deduced from those of graphite. Also note that ω_p respectively, approaches $2\gamma_0$ and $2.97\gamma_0$, at $q\to 0$ for finite N and $N=\infty$. For graphite with $N=\infty$, a detailed comparison between the calculated results and the experimental measurements[13,14] is given in Ref. 28.

IV. CONCLUDING REMARKS

In this work, we have calculated the π plasmons in a multiwall carbon nanotube, a single-wall carbon nanotube bundle with finite nanotubes, and graphite layers. The loss functions of the nanotube systems exhibit the most prominent π-plasmon peak as well as several interband plasmon peaks. The latter do not exist in graphite layers, mainly owing to the absence of 1D subbands. The π plasmon is an optical plasmon. Dependence on the chiral angle is negligible. However, the π plasmon is significantly affected by the transferred momentum, the transferred angular momentum, and the number of carbon nanotubes or graphite layers. The intertube or interlayer Coulomb interactions apparently enhance plasmon frequency and oscillator strength for increasing N.

A multiwall carbon nanotube can exhibit L-decoupled π plasmons. The π-plasmon frequency clearly increases as L grows. For the $L=0\,\pi$ plasmon, multiwall carbon nanotube completely corresponds to graphite layers, but not to a single-wall carbon nanotube bundle. The similarities between a multiwall carbon nanotube and a single-wall carbon nanotube bundle include $\omega_p=2\gamma_0$ at $q=0$ and the linear q dependence of ω_p at large q. However, there are several important differences between them. The radius dependence is negligible for a multiwall carbon nanotube, while it is strong for a single-wall carbon nanotube bundle. Moreover, the former exhibits stronger collective excitations, higher π-plasmon frequency, and relatively rapid increase of ω_p with q at small q.

The calculated results can explain the experimental mea-

surements, two kinds of plasmon modes in a multiwall nanotube,[2] the 5.8 eV π plasmon in a large single-wall nanotube bundle,[12] and the similarities or differences between a single-wall carbon nanotube bundle and a multiwall nanotube.[16] EELS can be utilized[36] to verify the predicted results: the q- and N-dependent π plasmons in the graphite-related systems, and the L-decoupled π plasmons in a multiwall nanotube. Only the π band is included in the present calculations. When the σ band is taken into account,[42] it is useful in understanding the overall excitation properties at $\omega=0-40$ eV, e.g., the $\pi+\sigma$ plasmon with $\omega_p>20$ eV.[11–16] This problem will be investigated in further studies.

ACKNOWLEDGMENTS

We thank R. Friedlein for communicating experimental results prior to publication. This work was supported in part by the National Science Council of Taiwan, Republic of China under Grant No. NSC 89-2112-M-006-011.

APPENDIX

The π-band structures of a graphite layer and a single-wall carbon nanotube are briefly reviewed here. A graphite sheet has two carbon atoms in a primitive cell. The Bloch states are described by two tight-binding functions built from the $2p_z$ orbitals $\phi_z(\mathbf{r}')$:

$$U_{i\mathbf{k}'}(\mathbf{r}')=C\sum_{\mathbf{R}_n} e^{i\mathbf{k}'\cdot(\mathbf{R}_n+\tau_i)}\phi_z(\mathbf{r}'-\mathbf{R}_n-\tau_i), \quad i=1,2. \tag{A1}$$

C is the normalization factor, $\mathbf{k}'$ is the 2D wave vector, and $\mathbf{R}_n$ is the lattice vector. τ_1 and τ_2 define the positions of the two basis atoms. The single-orbital nearest-neighbor tight-binding Hamiltonian is used to calculate the π band. The energy dispersions of a graphite layer, obtained by diagonalizing the Hamiltonian, are given by

$$E^{c,v}(k_{x'},k_{y'})=\pm\gamma_0\left[1+4\cos\left(\frac{3bk_{y'}}{2}\right)\cos\left(\frac{\sqrt{2}bk_{x'}}{2}\right)+4\cos^2\left(\frac{\sqrt{2}bk_{x'}}{2}\right)\right]^{1/2}, \tag{A2}$$

and the wave functions are

$$\Psi^{c,v}_{\mathbf{k}'}(\mathbf{r}')=\frac{1}{\sqrt{3}}\left(U_{1\mathbf{k}'}(\mathbf{r}')\mp\frac{H^*_{12}(k_{x'},k_{y'})}{|H_{12}(k_{x'},k_{y'})|}U_{2\mathbf{k}'}(\mathbf{r}')\right). \tag{A3}$$

The superscript $c(v)$ represents the antibonding π^* band (the bonding π band) above (below) the Fermi level $E_F=0$. γ_0 [$\sim$2.3–2.7 eV (Ref. 45)] is the nearest-neighbor resonance integral. $H_{12}=-\gamma_0\Sigma_{i=1}^{3}e^{-ik'\cdot r_i}$ is the nearest-neighbor Hamiltonian matrix element. The π band strongly depends on the direction of the wave vector. Energy vanishes at the corners (K and K') of the first Brillouin zone. Furthermore, $E^c=\gamma_0$ and $E^v=-\gamma_0$ for the middle point M between K and K'. The electronic excitations from the states near the M point are associated with the π plasmon.[28]

A similar tight-binding calculation is applied to a cylindrical carbon nanotube, but with the periodic boundary condition along the rolled (transverse) direction. A carbon nanotube samples the π-electron states of a graphite sheet, which satisfies the periodic boundary condition. The angle between the rolled direction (the x axis) and the x' axis is defined as the chiral angle θ.[22] The relationship between wave vectors (k_x,k_y) of a carbon nanotube and those $(k_{x'},k_{y'})$ of a graphite layer is described by

$$k_{x'}=k_x\cos\theta-k_y\sin\theta \tag{A4a}$$

and

$$k_{y'}=k_x\sin\theta+k_y\cos\theta. \tag{A4b}$$

Equations (A2) and (A3), together with the above transformation, describe the π band of a carbon nanotube. The axial wave vector k_y is confined within the first Brillouin zone. The transverse wave vector needs to satisfy the periodic boundary condition. It is given by $k_x=J/r$, where $J=1,2,...,N_u/2$; N_u is the number of atoms in a primitive unit cell. J is the angular momentum of electrons circulating the nanotube. It can serve as the subband index. The π-band structure has three main features. There are many 1D subbands with strong k_y dependence. The subbands are concave upward (downward) for $E^v(k_y=0)\leqslant-\gamma_0$ [$E^c(k_y=0)\geqslant\gamma_0$]. The subbands with $E^v(k_y=0)\sim-\gamma_0$ [$E^c(k_y=0)\sim\gamma_0$] correspond to the states near the M point of a graphite layer. They induce the π plasmon. Moreover, the density of states hardly depends on the chiral angle except at low energies. For an armchair (m,m) nanotube, the energy dispersions are given by

$$E^{c,v}(J,k_y)=\pm\gamma_0\left[1+4\cos\left(\frac{\sqrt{2}bk_y}{2}\right)\cos\left(\frac{J\pi}{m}\right)+4\cos^2\left(\frac{\sqrt{2}bk_y}{2}\right)\right]^{1/2}, \tag{A5}$$

where $J=1,2,\ldots,2m$.

*Electronic address: mflin@mail.ncku.edu.tw

[1] S. Iijima, Nature (London) **354**, 56 (1991).

[2] R. Kuzno, M. Terauchi, M. Tanaka, and Y. Saito, Jpn. J. Appl. Phys., Part 2 **33**, L1316 (1994).

[3] L. A. Bursill, P. A. Stadelmann, J. L. Peng, and S. Prawer, Phys. Rev. B **49**, 2882 (1994).

[4] Z. F. Ren *et al.*, Appl. Phys. Lett. **75**, 1086 (1999).

[5] T. Iwasaki, T. Motoi, and T. Den, Appl. Phys. Lett. **75**, 2044 (1999).

[6] S. Iijima and T. Ichihashi, Nature (London) **363**, 603 (1993).

[7] D. S. Bethune, C. H. Kiang, M. S. de Vries, G. Gorman, R. Savoy, J. Vazquez, and R. Beyers, Nature (London) **363**, 605 (1993).

[8] C. H. Kiang and W. A. Goddard III, Phys. Rev. Lett. **76**, 2515 (1996).

[9] A. Thess *et al.*, Science **273**, 438 (1996).

[10] C. Journet, W. K. Maser, P. Bernier, A. Loisean, M. Lamy de la Chapelle, S. Lefrant, P. Deniard, R. Lee, and J. E. Fischer, Nature (London) **388**, 756 (1997).

[11] P. M. Ajayan, S. Iijima, and T. Ichihashi, Phys. Rev. B **47**, 6859

(1993).
[12] R. Kuzuo, M. Terauchi, and M. Tanaka, Jpn. J. Appl. Phys. **31**, L1484 (1992).
[13] K. Zeppenfeld, Z. Phys. **243**, 229 (1971).
[14] U. Buchner, Phys. Status Solidi B **81**, 227 (1977).
[15] E. A. Taft and H. R. Philipp, Phys. Rev. **138**, A197 (1965).
[16] R. Friedlein, M. Knupfer, T. Pichler, M. S. Golden, K. Mukhopadhyay, T. Sugai, H. Shinohara, and J. Fink (unpublished).
[17] H. Ehrenreich and M. H. Cohen, Phys. Rev. **115**, 786 (1959).
[18] M. F. Lin, D. S. Chuu, C. S. Huang, Y. K. Lin, and K. W.-K. Shung, Phys. Rev. B **53**, 15 493 (1996).
[19] For the details of the dielectric function of an infinite carbon nanotube bundle see M. F. Lin and D. S. Chuu, Phys. Rev. B **57**, 10 183 (1998).
[20] T. Tsuzuku, Carbon **17**, 293 (1979).
[21] R. Saito, G. Dresselhaus, and M. S. Dresselhaus, J. Appl. Phys. **73**, 494 (1993).
[22] Y. K. Kwon and D. Tomanek, Phys. Rev. B **58**, 16 001 (1998).
[23] E. T. Jensen, R. E. Palmer, W. Allison, and J. F. Annett, Phys. Rev. Lett. **66**, 492 (1991); P. Laitenberger and R. E. Palmer, *ibid.* **76**, 1952 (1996).
[24] F. Bassani and G. Pastori Parravicini, Nuovo Cimento A **50**, 95 (1967).
[25] D. L. Greenaway, G. Herbeke, F. Bassani, and E. Tosatti, Phys. Rev. **178**, 1340 (1969).
[26] G. S. Painter and D. E. Ellis, Phys. Rev. B **1**, 4747 (1970).
[27] M. Tsukada, K. Nakao, Y. Umeura, and S. Nagai, J. Phys. Soc. Jpn. **32**, 54 (1972).
[28] For details of the response function of graphite see M. F. Lin and D. S. Chuu, Phys. Rev. B **55**, 13 961 (1997).
[29] R. Saito, M. Fujita, G. Dresselhaus, and M. S. Dresselhaus, Appl. Phys. Lett. **60**, 2204 (1992); Phys. Rev. B **46**, 1804 (1992).
[30] P. R. Wallace, Phys. Rev. **71**, 622 (1947).
[31] For details of the geometric structures of carbon nanotubes and graphite see M. F. Lin and K. W.-K. Shung, Phys. Rev. B **52**, 8423 (1995).
[32] M. F. Lin and K. W.-K. Shung, Phys. Rev. B **47**, 6617 (1993).
[33] C. Yannouleas, E. N. Bogachek, and U. Landman, Phys. Rev. B **50**, 7977 (1994); **53**, 10 225 (1996).
[34] B. Tanatar, Phys. Rev. B **55**, 1361 (1997).
[35] S. Das Sarma and J. J. Quinn, Phys. Rev. B **25**, 7603 (1982); P. Hawrylak, Phys. Rev. Lett. **59**, 485 (1987).
[36] C.-M. Grimaud, L. Siller, M. Andersson, and R. E. Palmer, Phys. Rev. B **59**, 9874 (1999).
[37] J.-C. Charlier and J.-P. Michenaud, Phys. Rev. Lett. **70**, 1858 (1993); A. Burian, J. C. Dore, H. E. Fischer, and J. Solan, Phys. Rev. B **59**, 1665 (1999).
[38] M. S. Dresselhaus and G. Dresselhans, Adv. Phys. **30**, 139 (1981).
[39] T. Pichler, M. Knupfer, M. S. Golden, J. Fink, A. Rinzler, and R. E. Smalley, Phys. Rev. Lett. **80**, 4729 (1998).
[40] C. T. White and J. W. Mintmire, Nature (London) **394**, 29 (1998).
[41] C. T. White, D. H. Robertson, and J. W. Mintwire, Phys. Rev. B **47**, 5485 (1993).
[42] J.-C. Charlier and Ph. Lambin, Phys. Rev. B **57**, 15 037 (1998).
[43] J. W. Mintwire, B. I. Dunlap, and C. T. White, Phys. Rev. Lett. **68**, 631 (1992).
[44] J. W. Mintwire and C. T. White, Phys. Rev. Lett. **81**, 2506 (1998).
[45] J. W. McClure, Phys. Rev. **104**, 666 (1956); J. C. Slonczewski *et al.*, *ibid.* **109**, 272 (1958); J.-C. Charlier *et al.*, Phys. Rev. B **46**, 4531 (1992); M. Tsukada *et al.*, J. Phys. Soc. Jpn. **32**, 54 (1972); J. Blinowski *et al.*, J. Phys. (Paris) **41**, 47 (1980).
[46] J. M. Cowley, P. Nikolaev, A. Thess, and R. E. Smalley, Chem. Phys. Lett. **265**, 379 (1997).
[47] S. Bandow, S. Asaka, Y. Saito, A. M. Rao, L. Grigorian, E. Richter, and P. C. Eklund, Phys. Rev. Lett. **80**, 3779 (1998).
[48] O. Jost, A. A. Gorbunov, W. Pompe, T. Pichler, R. Friedlein, M. Knupfer, M. Reibold, H.-D. Bauer, L. Dunsch, M. S. Golden, and J. Fink, Appl. Phys. Lett. **75**, 2217 (1999).